Available online at www.sciencedirect.com
ScienceDirect
Nuclear Medicine and Biology 36 (2009) 877–882
NUCLEAR MEDICINE AND BIOLOGY
www.elsevier.com/locate/nucmedbio

Validation of the calculation of the clearance rate constant (k_{mono}) of [^{11}C]acetate using parametric k_{mono} image for myocardial oxidative metabolism☆

Raihan Hussain, Takashi Kudo*, Testuya Tsujikawa, Masato Kobayashi, Yasuhisa Fujibayashi, Hidehiko Okazawa

Biomedical Imaging Research Center, University of Fukui, Fukui, Japan

Received 14 April 2009; received in revised form 9 June 2009; accepted 2 July 2009

Abstract

Introduction: The purpose of this study was to validate the calculation of myocardial oxidative metabolism rate using a parametric clearance rate constant (k_{mono}) image.
Methods: Fifteen subjects (seven volunteers, eight patients) were studied. Dynamic PET was acquired after intravenous injection of 700 MBq of [^{11}C]acetate. The clearance rate constant of [^{11}C]acetate (k_{mono}) was calculated pixel by pixel to generate the parametric k_{mono} image. The k_{mono} values from this image and those calculated from the dynamic image were compared in the same regions of interest (ROIs).
Results: Two different methods showed an excellent correlation except in the very low range. Regression equations were y=0.99x+0.0034 (r^2=0.86, P<001) and y=1.16x−0.0077 (r^2=0.87, P<001) in normal volunteer and patient groups, respectively, and y=1.07x−0.0019 (r^2=0.87, P<001) when combined.
Conclusions: Both methods exhibited similar values of k_{mono}. Parametric k_{mono} image may result in better visual understanding of regional myocardial oxidative metabolism.

Keywords: [^{11}C]Acetate; Parametric image; Oxidative metabolism; Cardiology; PET

1. Introduction

The noninvasive quantification of myocardial oxidative metabolism, particularly on a regional basis, is of critical importance in both cardiovascular investigation and clinical cardiology [1]. [^{11}C]Acetate avidly accumulates in the myocardium and then rapidly enters the tricarboxylic acid (TCA) cycle. The ^{11}C label is released as $^{11}CO_2$ at a rate proportional to the oxidation rate of the TCA cycle [2,3]. Since mitochondrial oxidation is tightly coupled to oxidative phosphorylation, and since other pathways for metabolism of acetate by the heart are modest, the oxidation of ^{11}C-acetate to $^{11}CO_2$ and subsequent clearance from the heart provide an index of myocardial oxidative metabolism [4]. This clearance of [^{11}C]acetate can be noninvasively determined using dynamic positron emission tomography (PET).

A clearance rate constant of [^{11}C]acetate, usually represented as k_{mono}, is usually measured at regions of interests (ROIs) on the dynamic count-based image and represented only as numerical values. But images instead of mere numerical values would be more useful in a clinical setting, especially in viability assessment. Thus, we developed a method for pixel-by-pixel generation of parametric k_{mono} image using logarithmic conversion of original dynamic counts. The purpose of this study was to validate a method to calculate k_{mono} using parametric k_{mono} images and to determine whether it is reliable or not in comparison with common ROI measurement methods on the dynamic count-based image.

☆ The authors attest that there is no financial support to be disclosed. There are no commercial associations that might pose a conflict of interest.

* Corresponding author. Tel.: +81 776 61 8491; fax: +81 776 61 8170.
E-mail addresses: raihan_h@yahoo.com (R. Hussain), tkudo@u-fukui.ac.jp (T. Kudo).

0969-8051/$ – see front matter © 2009 Elsevier Inc. All rights reserved.
doi:10.1016/j.nucmedbio.2009.07.002

2. Materials and methods

2.1. Subjects

Fifteen subjects, seven young male healthy volunteers (age range: 21 to 36 years; mean: 28.9±6.7 years) and eight patients (male=7, female=1; age range: 60 to 87 years; mean: 73.0±10.3 years) with coronary artery disease (CAD) with known myocardial infarction, were studied. The study was approved by the Ethics Committee of Fukui University Hospital. Written informed consent was obtained from each subject.

2.2. PET Procedures

PET scans were performed with a conventional whole-body PET scanner (ADVANCE, General Electric Medical System, Milwaukee, WI, USA), which permitted simultaneous acquisition of 35 image slices in a two-dimensional acquisition mode with interslice spacing of 4.25 mm [5]. Performance tests showed the intrinsic resolution of the scanner to be 4.6 to 5.7 mm in the transaxial direction and 4.0 to 5.3 mm in the axial direction. At first, a 10-min transmission scan was performed using ^{68}Ge/^{68}Ga for attenuation correction before the tracer administration. Then, about 700 MBq of [^{11}C]acetate was slowly administered intravenously over 30 s, and dynamic acquisition was done (18×5-, 7×30-, 5×60- and 5×120-s frames). Transaxial slices were collected in a matrix size of 128×128 pixels. The data were reconstructed with the filtered back-projection method using a Hanning filter with 6.0 mm full-width resolution at half maximum in the transaxial direction [6].

2.3. Calculation of k_{mono} values

To achieve the k_{mono} values, we applied two different methods. The first method used the original dynamic images. Data acquired between 3 and 8 min (when the activity was maximum) after administration of the tracer were summed together to form a composite image, which was only used to place ROIs in the proper position. A total of 24 ROIs (8×3 slices) were placed over the anterior, anteroseptal, septal, inferior, posterior and lateral walls of this image to obtain the time–activity curve (TAC). It is a well-known fact that k_{mono} obtained from the equation $q=Ae^{-kt}$ (where q=count/pixel per minute corrected for physical decay, $k=k_{mono}$ and t=time) [7] is an index of myocardial oxidative metabolism. A monoexponential function was fit to the TAC of these ROIs, and the values of k_{mono} were determined. The monoexponential fit begins at the time when the blood pool activity becomes low and TAC shows clear washout. In several reports, curve fitting begins at 2 to 4 min after injection. However, we found that excluding the data acquired before 400 s after injection usually resulted in better fitting. Considering this, we used data acquired 8–20 min after injection for the calculation of k_{mono}. Typical TAC and monoexponential fitting are presented in Fig. 1.

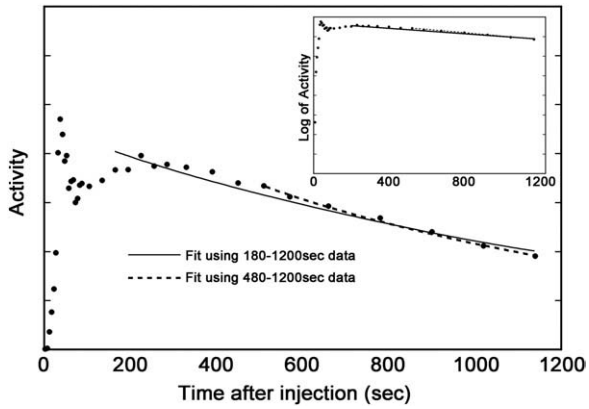

Fig. 1. Typical myocardial TAC of [^{11}C]acetate PET. Dots indicate actual time–activity curve. The solid line indicates exponential curve fitting using data 3–20 min after injection. The dashed line indicates fitting using data 8–20 min after injection. The inset is the same graph displayed with log scale.

The second method utilized the k_{mono} parametric image, which was constructed by calculating the pixel-by-pixel k_{mono} values using the same time frames used in the first method. Usually, exponential fitting is necessary to calculate k_{mono}. To simplify the pixel-by-pixel mathematical calculation, logarithmic conversion of image count was used. With this conversion, the equation previously described is converted to the following linear function: log q=log A ($-kt$). Thus, we can easily calculate the k_{mono} values pixel by pixel by linear fitting. The background noise and blood-pool region were masked to avoid unnecessary calculation of extramyocardial pixels. The generated parametric k_{mono} image was then smoothed using a 6-mm full width at half maximum Gaussian filter to reduce image noise. The average k_{mono} value of 24 ROIs in each subject was also calculated to perform subject-by-subject analysis.

2.4. Statistical analysis

The k_{mono} values measured with the two methods were correlated by linear least-square regression analysis. Differences between the k_{mono} values obtained with the two methods were also assessed by paired t test and the Bland–Altman plot method. All values were expressed as means±S. D. $P<.05$ was considered statistically significant. Statistical analysis was performed using the Statistica 06 package (Statsoft, Tulsa, OK, USA).

3. Results

3.1. Comparison of k_{mono} values

Fig. 2 shows the serial images from count-based reconstruction at the mid-ventricular level after administration of [^{11}C]acetate in normal (upper row) and infarcted myocardium (bottom row). Fig. 3 shows the corresponding k_{mono} images of the same subject.

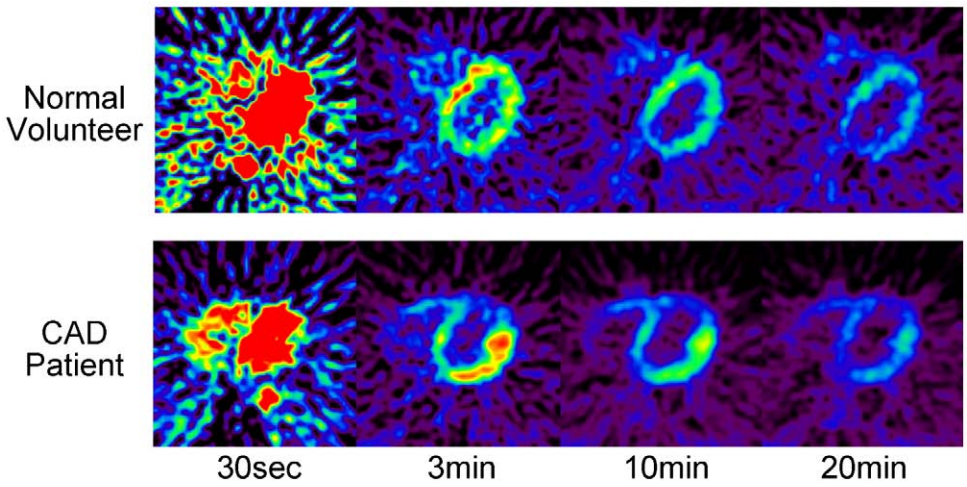

Fig. 2. Serial dynamic images from count-based reconstruction at the mid-ventricular level in normal myocardium (top row) and infarction in the apical anterior wall (bottom row). Approximately 700 MBq of [^{11}C]acetate was injected and the heart was imaged starting at the time of injection for 20 min.

Averages of the k_{mono} values in each subject obtained by the two different methods showed an excellent correlation. The k_{mono} values measured with parametric images were 0.061±0.014, and those measured with dynamic images were 0.063±0.014. The coefficient of determination (r^2) was 0.95 (P<.001), and the slope of the regression equation was very close to the line of identity (slope=1.008) (Fig. 4).

The k_{mono} values in each ROI were also compared (Fig. 5). Those obtained by the two different methods showed a slight but significant difference when each ROI was analyzed (0.061±0.018 vs. 0.063±0.020, P<.01 for the parametric k_{mono} image and dynamic image, respectively). An excellent correlation was found between the two methods except in the very low range (r^2=0.87, slope=1.07, P<.001). When normal volunteers and CAD patients were separately analyzed, the k_{mono} values were 0.065±0.019 vs. 0.068±0.021 (P<.01, normal group) and 0.057±0.015 vs. 0.058±0.019 (P<.01, CAD group), obtained from the parametric k_{mono} image and dynamic image, respectively. Correlation was still excellent even when normal volunteer and CAD groups were analyzed separately (r^2=0.86, slope=0.99, P<.001 for the normal volunteer group; r^2=0.87, slope=1.16, P<.001 for the CAD group).

3.2. Bland-Altman analysis

The Bland–Altman plot between the k_{mono} values obtained from the two methods is presented in Fig. 6. When all the ROIs were analyzed separately, the plot still

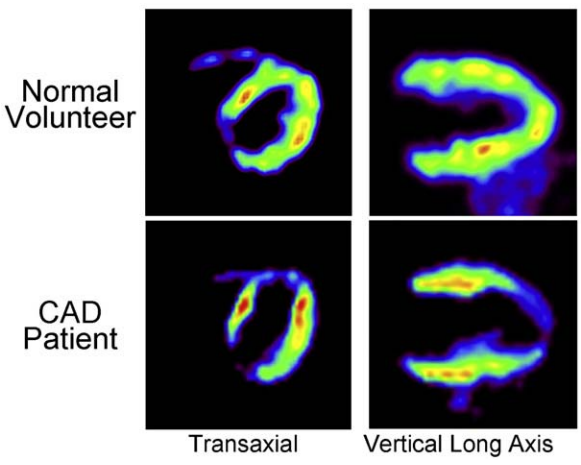

Fig. 3. The parametric k_{mono} images of the same subjects presented in Fig. 2 (left column) and reoriented into vertical long axis view (right column). Note that the low k_{mono} value is visible on the image of a CAD patient. To create these parametric images, approximately 700 MBq of [^{11}C]acetate was injected and the heart was imaged starting at the time of injection for 20 min.

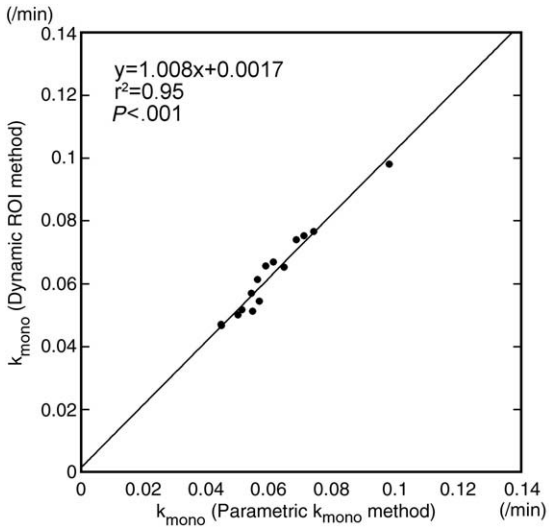

Fig. 4. The averaged k_{mono} values in each subject are plotted in a scatter chart with k_{mono} from a parametric image (ROIs) along the x-axis and from a dynamic image along the y-axis. The r^2 values, P values and equations are shown in the graph.

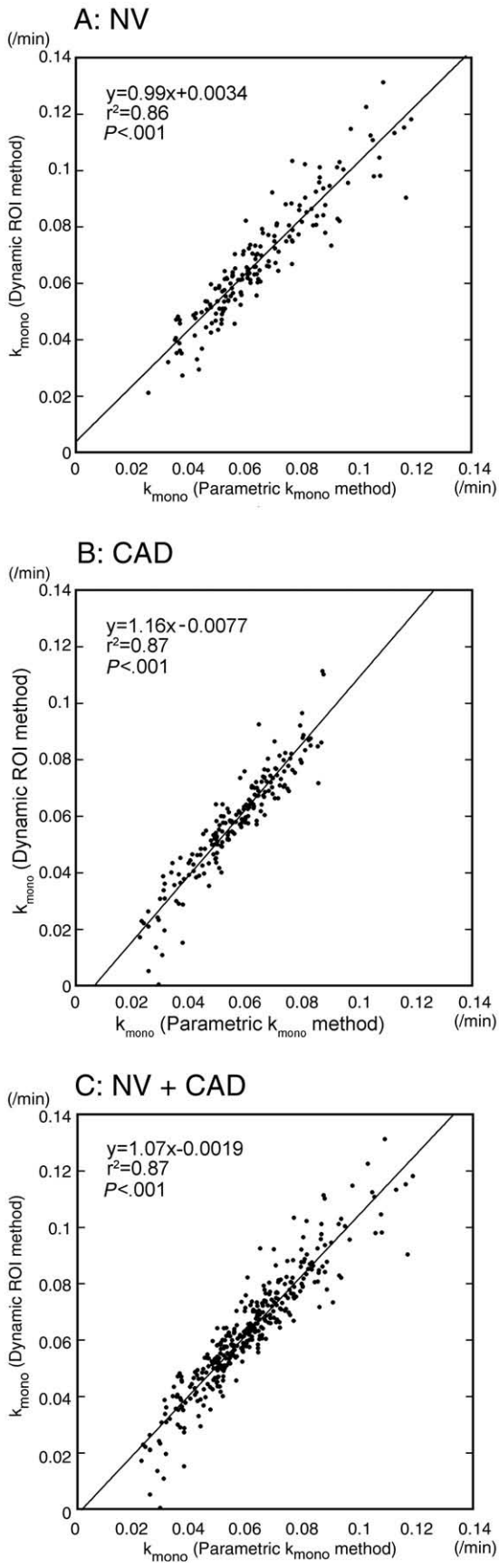

showed good agreement between the two measurements although it showed slightly strained distribution in the very low range, suggesting that the parametric k_{mono} image tended to show higher values than the ROI method in the very low range of k_{mono}.

4. Discussion

The current study shows that k_{mono} calculated on a pixel-by-pixel basis using logarithmic conversion of original dynamic counts and that obtained with the help of monoexponential fitting of the dynamic TACs of raw count data over the same ROIs have very good correlation. With this technique, parametric images of k_{mono} can be created reliably and easily. This k_{mono} parametric image can provide an easy visual clue for assessing myocardial metabolism, which is required in daily practice such as viability assessment. The visual assessment of viability using flow/metabolism mismatch criteria becomes possible with a single [^{11}C]acetate PET acquisition. The only exception was in the very low range, where parametric k_{mono} values tend to be higher (overestimated) than dynamic k_{mono} values. In normal subjects, homogenous clearance of [^{11}C]acetate throughout the myocardium was seen on the parametric k_{mono} image, whereas in patients with myocardial infarction, it was diminished in the infracted zones which is indicative of diminished myocardial oxidative metabolism as reported previously [7].

[^{11}C]Acetate PET permits the evaluation of myocardial oxidative metabolism which provides important information about cardiac disease [8]. One of the most important issues in clinical nuclear cardiology is the assessment of myocardial viability. For the myocardial viability assessment, flow metabolism mismatch detected with FDG-PET under glucose loading (and perfusion imaging) is considered the gold standard [9–12]. However, FDG imaging has several difficulties; for example, it requires feeding status control and has poor image quality in diabetic patients. [^{11}C]Acetate has been proposed as an alternative marker with minimal substrate dependency [11]. ^{11}C-Acetate is superior to FDG because it does not require feeding status control and is easily applicable to diabetic patients. It has been reported that viable segments after myocardial infarction on FDG-PET have preserved oxidative metabolism [13,14]. Additionally, a study reported that the segments without contractile reserve but with preserved glucose metabolism show a reduction in the oxidative metabolic response to stress [15], which suggests superior specificity of [^{11}C] acetate in viability assessment.

Fig. 5. The k_{mono} values are plotted in a scatter chart with k_{mono} from a parametric image along the x-axis and from a dynamic image along the y-axis. The r^2 values, P values and equations are shown in (A) normal myocardium, (B) myocardial infarction and (C) normal myocardium and myocardial infarction combined together.

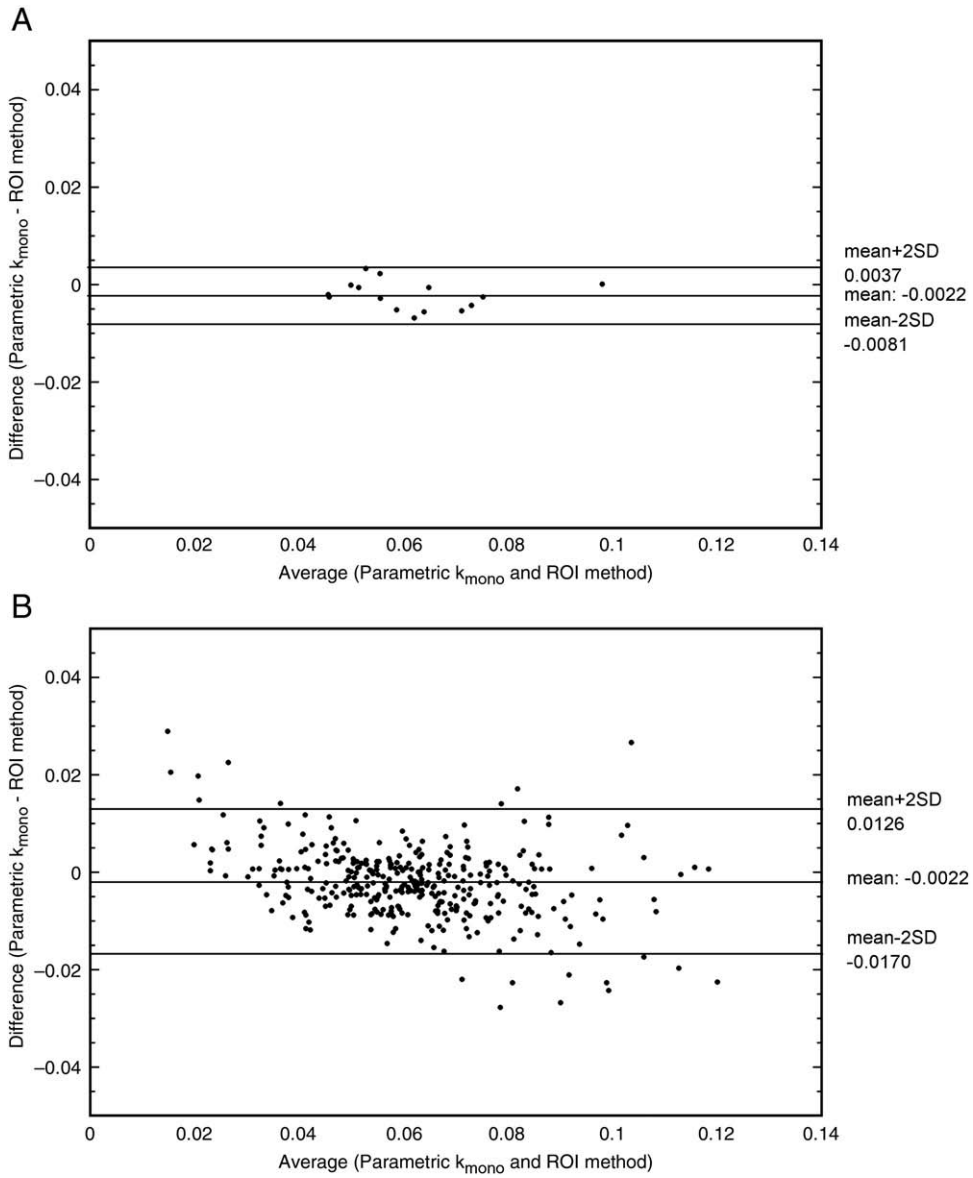

Fig. 6. Bland–Altman plot comparing the two methods. The averaged k_{mono} in each subject shows excellent agreement between the two methods without systematic deviation from 0 (Panel A). When each ROI is analyzed separately (Panel B), the Bland–Altman plot shows a trend in which k_{mono} values measured from parametric k_{mono} images tend to be higher than those measured from dynamic images in very low k_{mono} range. There is a minor but significant bias from 0.

To assess the viability, visual inspection is usually performed, especially when flow/metabolism mismatch criteria are used. So representing k_{mono} in numerical values only is not sufficient: representing in image format is preferred. Clinicians rely extensively on visual judgment, and parametric k_{mono} image could have an added advantage in this respect. The imaging guidelines from the American Society of Nuclear Cardiology recommend combined evaluation of perfusion and FDG images for viability assessment. This comparison is usually performed with qualitative image comparison [16]. Thus, parametric images of biological processes have been shown to facilitate quantitative analysis in the clinical environment [17,18].

[^{11}C]Acetate also allows accurate quantification of myocardial perfusion at rest as well as under stress conditions [19]. We previously reported that quantitative parametric image of myocardial perfusion is easily generated using the early-phase dynamic image of [^{11}C]acetate PET [20]. So it is attractive as a single-tracer technique that yields quantitative data and images on perfusion and metabolism and thus may help curtail the use of double-tracer studies [11].

Our method of creating k_{mono} parametric images showed a good correlation with k_{mono} measured on original dynamic image using the ROI and TAC method, except in the very low range, as mentioned before. These areas corresponded to known areas of infarction, where the oxidative metabo-

lism was negligible and possessed very low counts. This low-count statistic might be a cause of error on calculation. However, both methods gave values far below the normal range; so, clinically, this difference seems to be of no importance. We noted from the paired *t* test that there was a slight systematic underestimation of k_{mono} obtained from the parametric k_{mono} image compared to that obtained from the ROI method. Because pixel-by-pixel calculation is very susceptible to noise, we performed image smoothing for k_{mono} parametric image generation. This smoothing might have resulted in slight underestimation. However, the amount of underestimation was only about 3.7%. Thus, we believe that it should not cause any problem as the underestimation is not random, but is systematic.

5. Conclusion

Myocardial acetate clearance rate constant obtained from parametric image and that obtained from the ROI method on dynamic image in healthy volunteers as well as in patient groups exhibited similar values. Moreover, the parametric k_{mono} image may result in better understanding of regional myocardial oxidative metabolism than using just the k_{mono} numerical values. With the use of parametric k_{mono} images, visual inspection of metabolism is easily performed in clinical practices such as viability assessment.

References

[1] Beanlands R, Wolpers HG, Gropler RJ. Quantification of myocardial oxygen consumption using C-acetate. In: Schwaiger M, editor. Cardiac Positron Emission Tomography. Norwell: Kluwer Academic Publishers; 1996. p. 297–309.

[2] Ng CK, Huang SC, Schelbert HR, Buxton DB. Validation of a model for [1-^{11}C]acetate as a tracer of cardiac oxidative metabolism. Am J Physiol 1994;266:H1304–15.

[3] Lear JL. Relationship between myocardial clearance rates of carbon-11-acetate-derived radiolabel and oxidative metabolism: physiologic basis and clinical significance. J Nucl Med 1991;32:1957–60.

[4] Miller TR, Wallis JW, Geltman EM, Bergmann SR. Three-dimensional functional images of myocardial oxygen consumption from positron tomography. J Nucl Med 1990;31:2064–8.

[5] DeGrado TR, Turkington TG, Williams JJ, Stearns CW, Hoffman JM, Coleman RE. Performance characteristics of a whole-body PET scanner. J Nucl Med 1994;35:1398–406.

[6] Okazawa H, Takahashi M, Hata T, Sugimoto K, Kishibe Y, Tsuji T. Quantitative evaluation of myocardial blood flow and ejection fraction with a single dose of (13)NH(3) and gated PET. J Nucl Med 2002;43: 999–1005.

[7] Walsh MN, Geltman EM, Brown MA, Henes CG, Weinheimer CJ, Sobel BE, et al. Noninvasive estimation of regional myocardial oxygen consumption by positron emission tomography with carbon-11 acetate in patients with myocardial infarction. J Nucl Med 1989; 30:1798–808.

[8] Beanlands RS, Nahmias C, Gordon E, Coates G, deKemp R, Firnau G, et al. The effects of beta(1)-blockade on oxidative metabolism and the metabolic cost of ventricular work in patients with left ventricular dysfunction: a double-blind, placebo-controlled, positron-emission tomography study. Circulation 2000;102:2070–5.

[9] Baer FM, Voth E, Deutsch HJ, Schneider CA, Schicha H, Sechtem U. Assessment of viable myocardium by dobutamine transesophageal echocardiography and comparison with fluorine-18 fluorodeoxyglucose positron emission tomography. J Am Coll Cardiol 1994;24: 343–53.

[10] Barrington SF, Chambers J, Hallett WA, O'Doherty MJ, Roxburgh JC, Nunan TO. Comparison of sestamibi, thallium, echocardiography and PET for the detection of hibernating myocardium. Eur J Nucl Med Mol Imaging 2004;31:355–61.

[11] Gropler RJ, Geltman EM, Sampathkumaran K, Perez JE, Schechtman KB, Conversano A, et al. Comparison of carbon-11-acetate with fluorine-18-fluorodeoxyglucose for delineating viable myocardium by positron emission tomography. J Am Coll Cardiol 1993;22: 1587–97.

[12] Bax JJ, Poldermans D, Elhendy A, Boersma E, Rahimtoola SH. Sensitivity, specificity, and predictive accuracies of various noninvasive techniques for detecting hibernating myocardium. Curr Probl Cardiol 2001;26:147–86.

[13] Gropler RJ, Siegel BA, Sampathkumaran K, Perez JE, Sobel BE, Bergmann SR, et al. Dependence of recovery of contractile function on maintenance of oxidative metabolism after myocardial infarction. J Am Coll Cardiol 1992;19:989–97.

[14] Hata T, Nohara R, Fujita M, Hosokawa R, Lee L, Kudo T, et al. Noninvasive assessment of myocardial viability by positron emission tomography with ^{11}C acetate in patients with old myocardial infarction. Usefulness of low-dose dobutamine infusion. Circulation 1996;94: 1834–41.

[15] Yoshinaga K, Katoh C, Beanlands RS, Noriyasu K, Komuro K, Yamada S, et al. Reduced oxidative metabolic response in dysfunctional myocardium with preserved glucose metabolism but with impaired contractile reserve. J Nucl Med 2004;45:1885–91.

[16] Machac J, Bacharach SL, Bateman TM, Bax JJ, Beanlands R, Bengel F, et al. Positron emission tomography myocardial perfusion and glucose metabolism imaging. J Nucl Cardiol 2006;13:e121–51.

[17] Choi Y, Hawkins RA, Huang SC, Gambhir SS, Brunken RC, Phelps ME, et al. Parametric images of myocardial metabolic rate of glucose generated from dynamic cardiac PET and 2-[^{18}F]fluoro-2-deoxy-D-glucose studies. J Nucl Med 1991;32:733–8.

[18] Choi Y, Huang SC, Hawkins RA, Kuhle WG, Dahlbom M, Hoh CK, et al. A simplified method for quantification of myocardial blood flow using nitrogen-13-ammonia and dynamic PET. J Nucl Med 1993;34: 488–97.

[19] van den Hoff J, Burchert W, Borner AR, Fricke H, Kuhnel G, Meyer GJ, et al. [1-(11)C]Acetate as a quantitative perfusion tracer in myocardial PET. J Nucl Med 2001;42:1174–82.

[20] Kudo T, Hata T, Kagawa S, Kishibe Y, Iwasaki J, Nakano A, et al. Simple quantification of myocardial perfusion by pixel-by-pixel graphical analysis using carbon-11 acetate: comparison of the K-complexes of carbon-11 acetate and nitrogen-13 ammonia. Nucl Med Commun 2008;29:679–85.